Magnetic losses in soft ferrites

Samuel Dobák[1*], Cinzia Beatrice[2], Vasiliki Tsakaloudi[3], and Fausto Fiorillo[2]

[1] Institute of Physics, Faculty of Science, P.J. Šafárik University, 04154 Košice, Slovakia.
[2] Istituto Nazionale di Ricerca Metrologica-INRIM, 10135 Torino, Italy.
[3] Center for Research and Technology Hellas CERTH, 57001 Thermi-Thessaloniki, Greece
* Correspondence: f.fiorillo@inrim.it Tel.: +39 011 3919841

Supplementary material

Graphs and comments are provided regarding materials preparation, physical characterization, measuring methods, experimental results, and theoretical modeling.

The starting Mn-Zn ferrite powder was prepared by the conventional ceramic method of solid state reaction. The high purity raw materials (Merck), consisting of 70 wt % Fe_2O_3, 24 wt % MnO and 6 wt % ZnO, were weighed in the right proportions to give a batch of 500 g and were dry-mixed using a lab mixer. The oxides mixture was prefired at 800^0C in air and the crystal structure of the pre-fired powder was determined by X-ray Diffraction. Typical dopants, such as Nb_2O_5 and CaO were introduced into the pre-fired powder and ball milling was applied for 8 hours, using steel vessels. The particle size distribution of the milled powder was determined by laser scattering (Malvern Mastersizer S). Roll granulation of the milled powder was performed using a rotating drum with the addition of 0.2 wt % of aqueous solution of polyvinyl alcohol (Merck, Analytical Grade, MW72000). The Mn-Zn ferrite granulated powders were pressed using an isostatic hydraulic press and the toroidal specimens of external diameter of 16.8 mm, internal diameter of 8.4 mm and height of 6 mm were measured to have a press density of 2.90±0.02 g/cm^3. Sintering was performed in specially constructed programmable kilns following the oxygen partial pressure equilibrium proposed by Morineau and Paulus. Different sintering schedules were performed at the temperatures T_s = 1325 °C, 1340 °C, and 1360 °C for times t_s = 3 hours, 5 hours, and 7 hours at top temperature. The Archimedes' method was followed to measure the sinter density of the final ring specimens. These had outside diameter (D_o), inside diameter (D_i) and thickness (d) in the ranges: 14.54 mm – 14.64 mm (D_o), 9.28 mm – 9.36 mm (D_i), 4.86 mm – 5.16 mm (d). The magnetic path length was calculated as $l_m = \pi(D_o - D_i)/\ln(D_o/D_i)$. The polycrystalline microstructure of the sintered specimens was evaluated by Scanning Electron Microscopy (SEM-Jeol 6300) on the ground, polished and chemically etched toroidal specimens coming from each of the sintering trials.

The SEM investigation shows broadening distribution and larger mean value <s> of the grain size on increasing the sintering temperature T_s, as illustrated by the example shown in Fig. S1. Homogeneous grain growth is observed for T_s = 1325 °C and T_s = 1340 °C with some residual porosity. Increasing T_s to 1360 °C somewhat exceeds the optimal conditions for homogeneous grain growth and incipient secondary re-crystallization is observed. This is especially important upon the 7-hour treatment, as demonstrated by the corresponding irregular grain size distribution shown in Fig. S2.

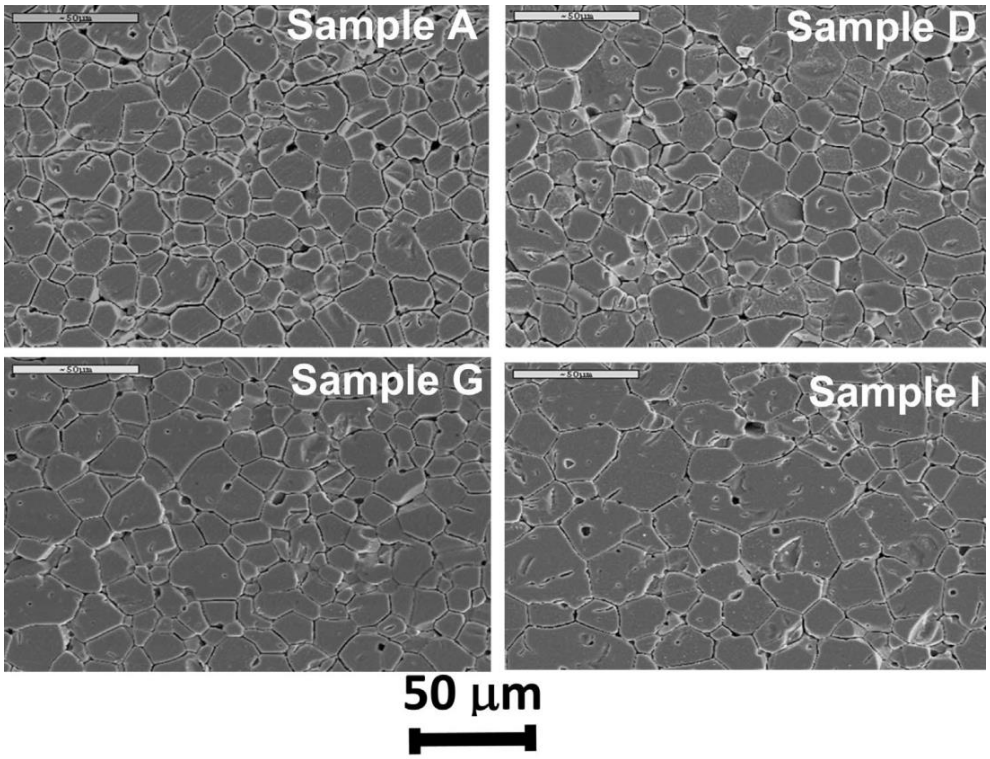

Figure S1. SEM micrographs of the grain structure of the Mn-Zn ferrites following different sintering treatments: A) 1325 °C -3 hours, D) 1340 °C-3hours; G) 1360 °C-3hours; I)1360 °C-7 hours.

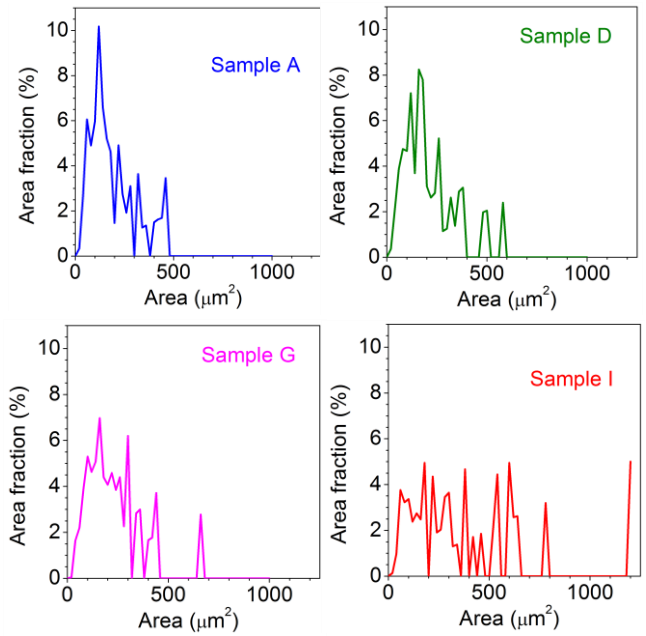

Figure S2. Distribution of the area fraction of the grains obtained by SEM analysis.

Mn-Zn ferrite powders were also prepared under a defined doping scheme with CaO and Nb_2O_5 and further addition of CoO in concentrations ranging between 0 – 6000 ppm, step 1000 ppm. Ring specimens of outside diameter about 14 mm were obtained by compaction of the milled and

granulated powders. Sintering of the samples was made at T = 1325 °C, under appropriate partial oxygen pressure, followed by microstructural analysis by Scanning Electron Microscopy (JEOL 6300) and density measurement by Archimedes' method. The average grain size ranged between 10.7 μm and 13.1 μm and the density slightly increased from 4920 kg/m^3 (CoO = 0) to 5040 kg/ m^3 (CoO = 6000 ppm). The real ρ′(f) and imaginary ρ′′ (f) resistivity components were obtained by the standard four-point electrical impedance measurements up to f = 10 MHz. The found dependence of ρ′(f) and ρ′′(f) on frequency is consistent with the conventional equivalent RC circuit lumping the electrical properties of the semiconducting grains and their insulating layer. The DC (grain boundary layer) and high-frequency (grain interior) resistivities are moderately affected (up to 20 – 30 %) by CoO doping, with ρ′′(f) becoming negligible with respect to ρ′(f) beyond about 10 MHz. At such frequencies, the conductivity in Eq. (1) $\sigma'(f) = \frac{\rho'(f)}{\rho'(f)^2+\rho''(f)^2} \sim \frac{1}{\rho'(f)}$ becomes quite constant and little dependent on temperature. Selected physical and magnetic properties of the developed ferrites and their dependence on CoO doping are provided in Tables 1 and 2.

TABLE S1 – Physical parameters of the investigated CoO-doped Mn-Zn ferrites.

Sample	CoO (ppm)	Grain size <s> (μm)	Density δ (kg/m^3)	DC resistivity ρ_{DC} (Ω m)	Real resistivity at 10 MHz ρ'_{10MHz} (Ω m)	Imaginary resistivity at 10 MHz ρ''_{10MHz} (Ω m)
A0	0	10.8	4.92	4.42	0.0130	-0.0076
A1	1000	10.7	4.98	5.08	0.0170	-0.0080
A2	2000	11.9	4.98	5.39	0.0165	-0.0073
A3	3000	12.2	5.01	5.52	0.0195	-0.0069
A4	4000	13.1	4.98	5.66	0.0185	-0.0069
A5	5000	10.8	5.01	5.9	0.0154	-0.0076
A6	6000	11.1	5.04	6.1	0.0137	-0.0096

TABLE S2 – Selected magnetic parameters in the Mn-Zn ferrites versus CoO content at room temperature. J_s ≡ saturation polarization; $\mu_{r,2mT}$ ≡ initial permeability at 100 kHz; $\mu'_{r,100mT}$ ≡ real permeability at 100 mT and 100 kHz; W_{100mT} ≡ Energy loss at 100 mT and 100 kHz; $\mu_{DC,rot}$ ≡ DC rotational permeability; K ≡ calculated average anisotropy constant.

Sample	CoO (ppm)	J_s (T)	$\mu_{r,2mT}$	$\mu'_{r,100mT}$	W_{100mT}(J/m^3)	$\mu_{DC,rot}$	K (J/m^3)
A0	0	0.540	2230	4199	1.540	2110	36.68
A1	1000	0.534	2258	3889	1.310	2070	36.56
A2	2000	0.529	2480	3906	1.020	2210	33.61
A3	3000	0.524	2690	3742	0.845	2380	30.38
A4	4000	0.522	2555	3401	0.687	2300	31.44
A5	5000	0.532	2070	3712	1.185	1713	43.85
A6	6000	0.536	1385	3100	2.100	1190	64.07

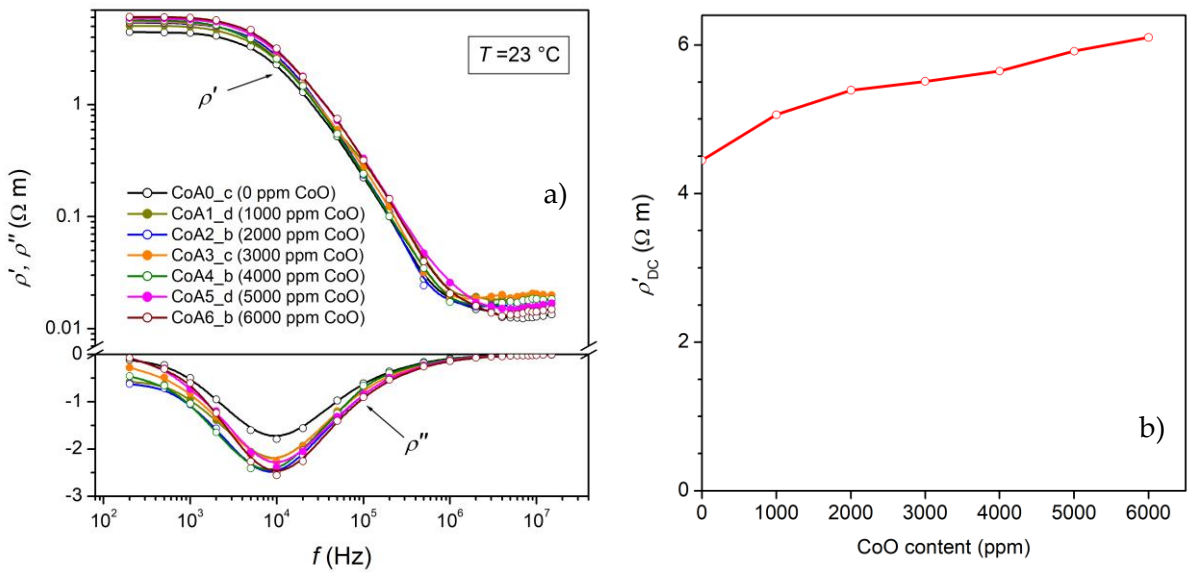

Figure S3. a) Real ρ′(*f*) and imaginary ρ′′(*f*) resistivity components measured between DC and 10 MHz in Mn-Zn ferrites endowed with different CoO content. The results point to a capacitive components originating from the dielectric properties of the grain boundaries. b) The DC resistivity increases monotonically with the CoO content.

The magnetic characterization is performed up to 10 MHz by fluxmetric measurements, based on the use of a calibrated hysteresisgraph-wattmeter. The primary and secondary windings, their layout, and the connecting cables ensure minimum spurious effects due to the stray capacitances. The high-frequency measurements, from a few hundred kHz to 1 GHz, are covered by a transmission line method, where the impedance of the ferrite sample placed at the bottom of a shorted coaxial cable is obtained by measuring the reflection scattering parameter by an Agilent 8753A Vector Network Analyzer (VNA, 10 mW irradiated power).

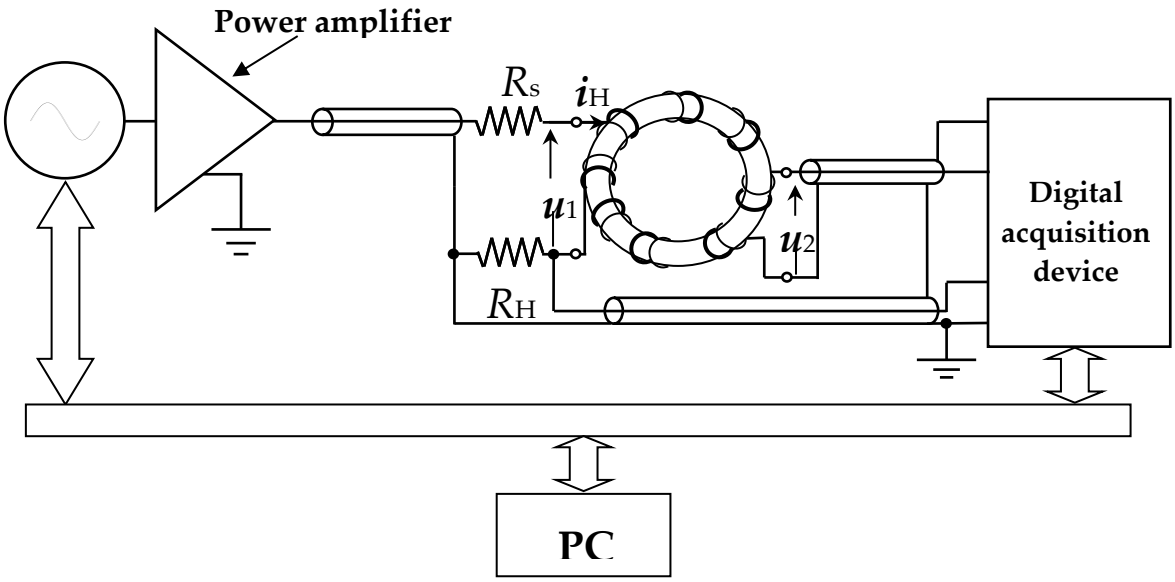

Figure S4. Magnetic characterization of ferrite rings by the fluxmetric method.

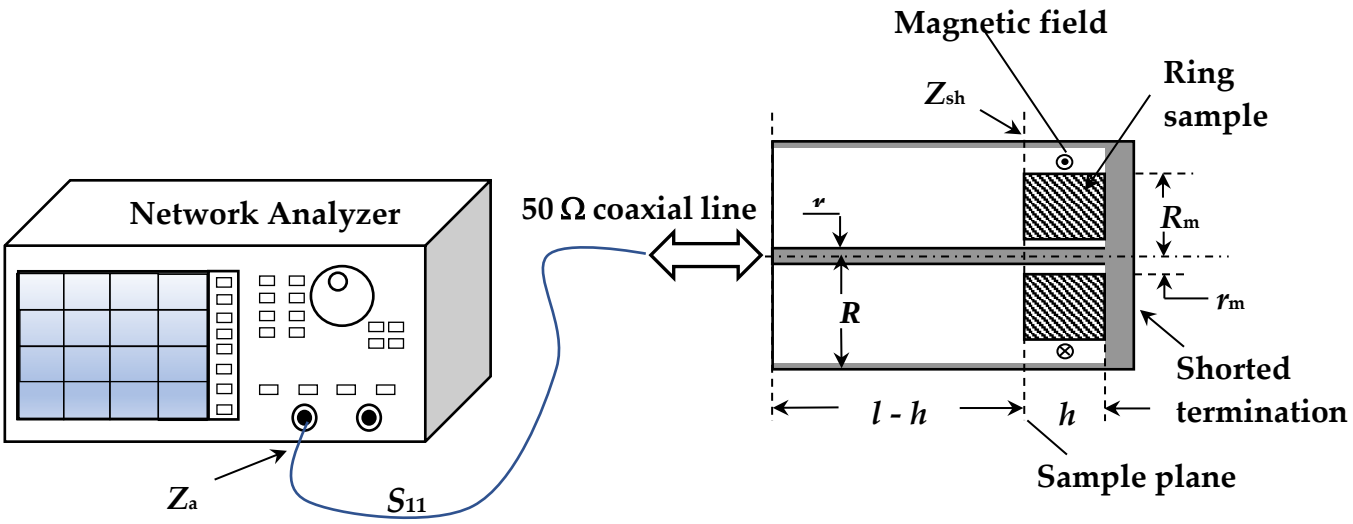

Figure S5. Measurement of the scattering parameter S_{11} and its dependence on the complex permeability of the ferrite ring sample by a Vector Network Analyzer. The sample is placed at the bottom of a shorted line. The complex permeability is obtained from the sample impedance $Z = \frac{1+S_{11}}{1-S_{11}} Z_0$, where Z_0 is the characteristic impedance of the line.

The energy loss per unit volume is obtained as

$$W(f) = \pi J_p^2 \mu'' / (\mu'^2 + \mu''^2) = \pi H_p^2 \mu'' \quad , \qquad [\mathrm{J/m^3}]$$

for a given peak polarization value J_P (or peak field value H_P).

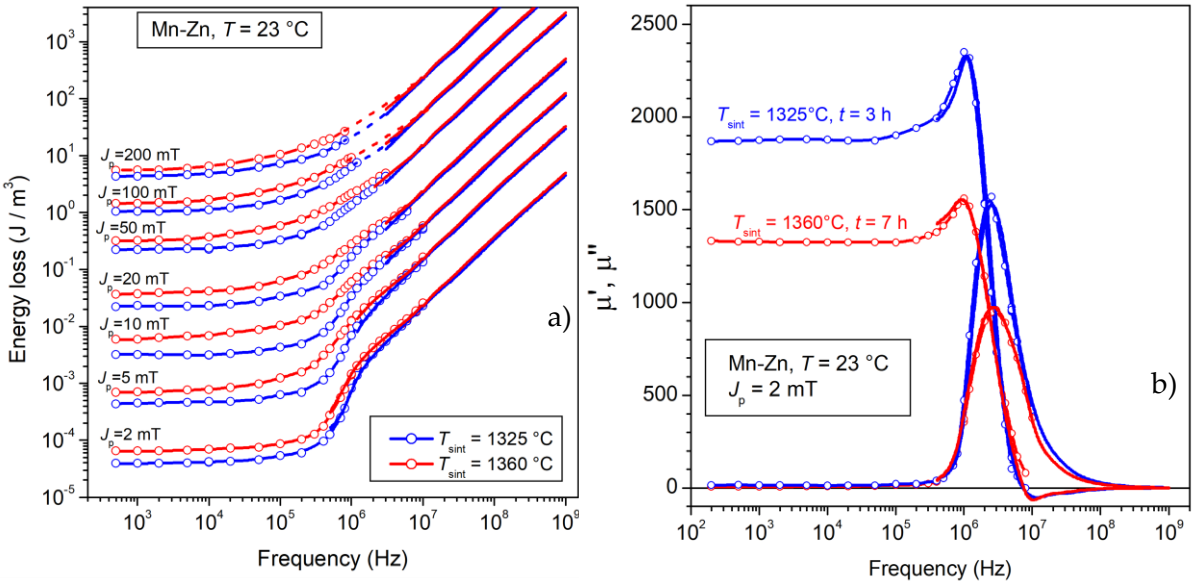

Figure S6. The properties of ferrite ring samples sintered at 1325 °C and 1360 °C are compared in this figures. a) Energy loss up to 1 GHz for J_P ranging between 2 m T and 200 mT. b) The real $\mu'(f)$ and imaginary $\mu''(f)$ initial permeabilities decrease upon sintering at the higher temperature of 1360 °C.

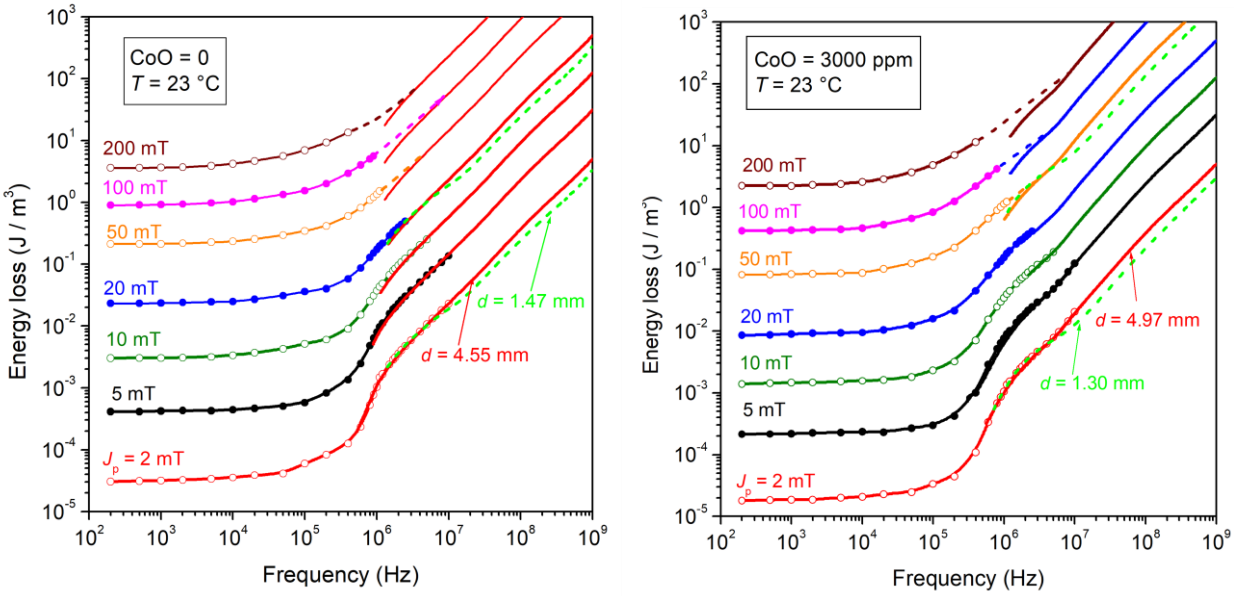

Figure S7. Energy loss $W(f)$ versus frequency in an undoped and an optimally doped Mn-Zn ferrites. The symbols indicate the results of the fluxmetric measurements. The continuous lines, obtained by the transmission line measurements, cover the upper frequency band, till 1 GHz. The overlapping region, belonging to both methiods, is apparent . Eddy currents can provide an extra-contribution to the loss beyond a few MHz in sufficiently thick samples, as signalled by the bifurcating behaviour of $W(f)$ at high frequencies.

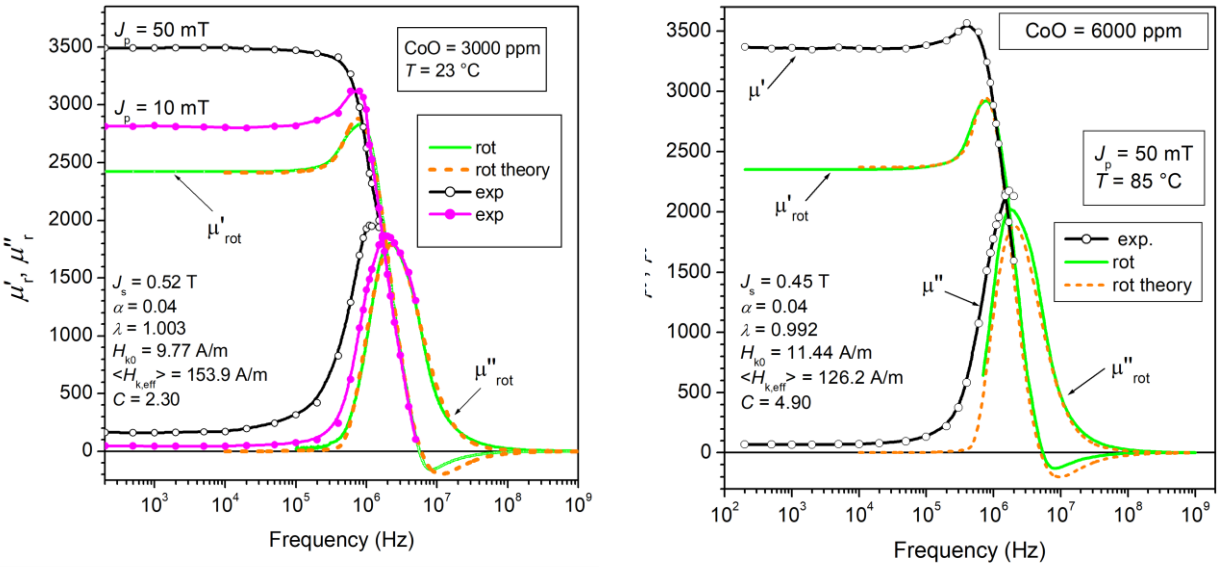

Figure S8. The rotational contributions $\mu'_{rot}(f)$ and $\mu''_{rot}(f)$ are singled out from the measured permeability in CoO-doped Mn-Zn ferrites. These quantities are theoretically predicted starting from the Landau-Lifshitz equation, which is applied under the assumption that the polycrystalline material is the seat of internal anisotropy fields distributed in direction and amplitude.

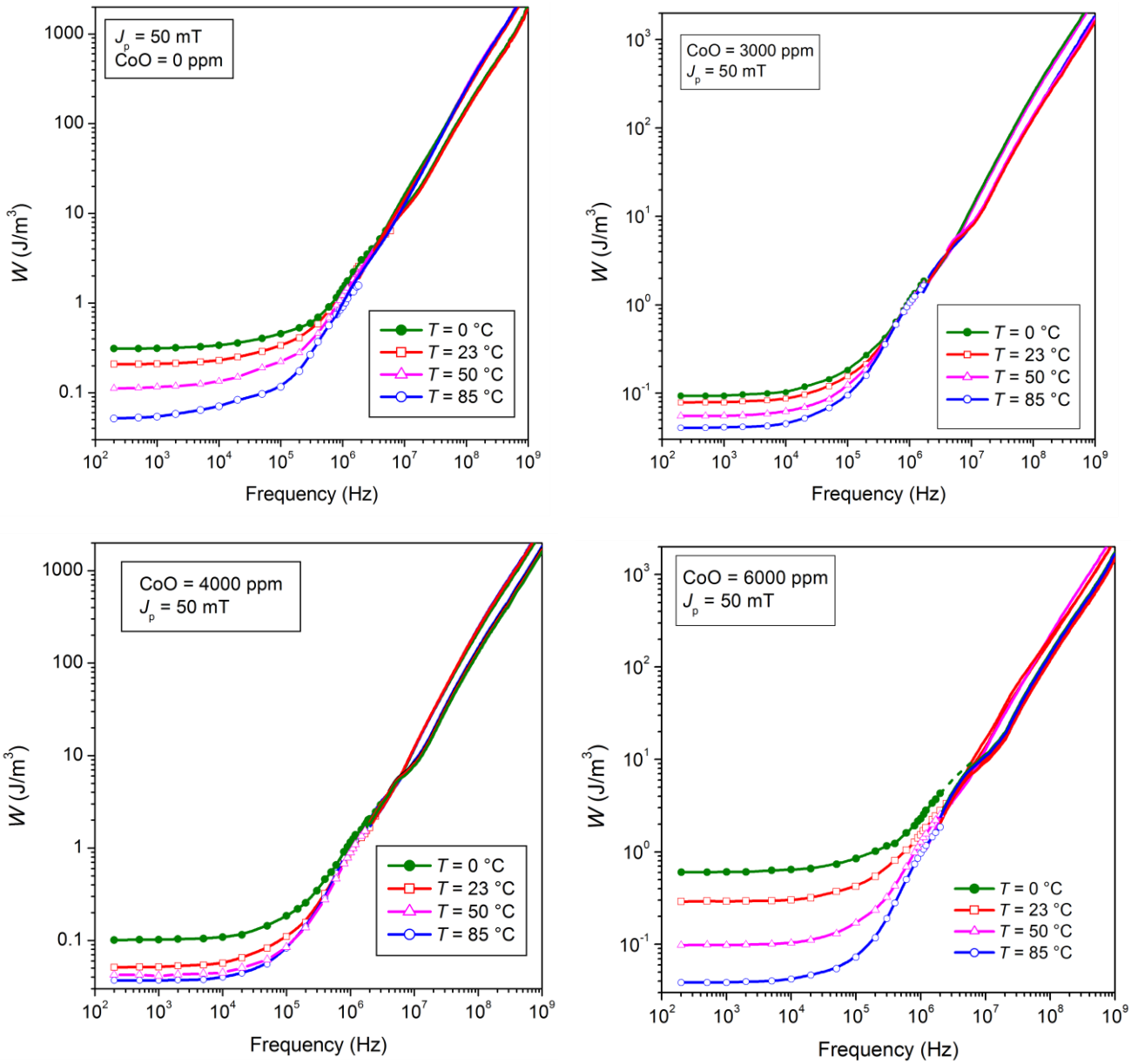

Figure S9. Energy loss $W(f)$ at J_P = 50 mT at different temperatures and different doping levels. Bifurcation at high frequencies separates the response of the as-obtained samples (thickness ~ 5 mm) from that of the same samples after thinning (thickness ~ 1.4 mm).

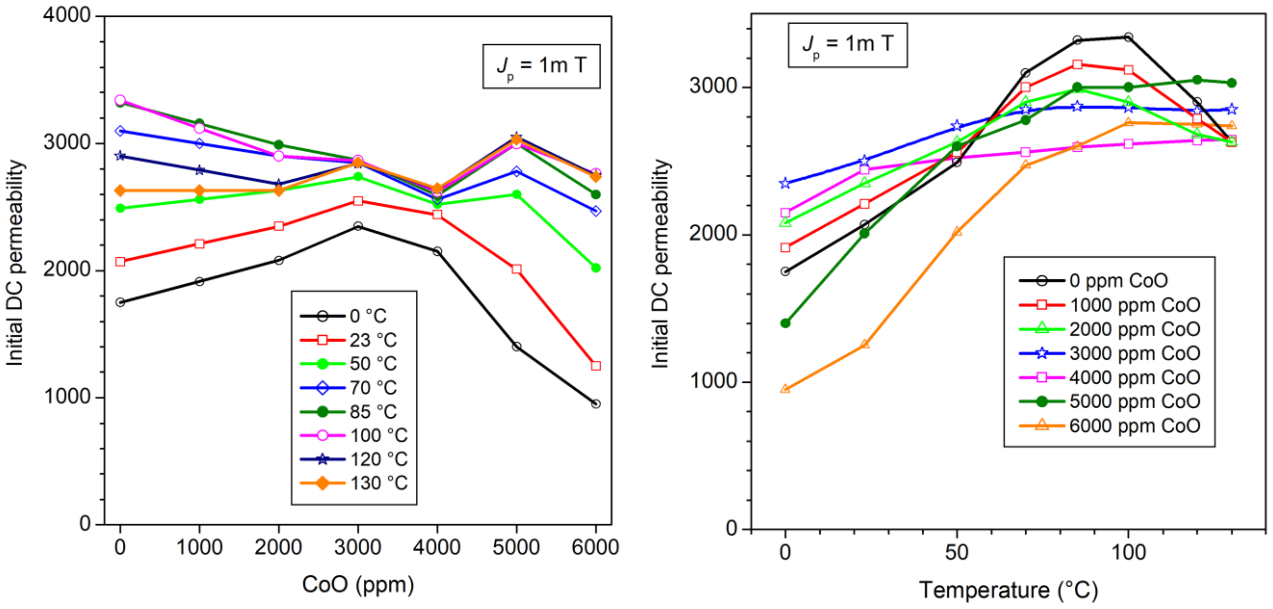

Figure S10. The optimally CoO-doped Mn-Zn ferrites (CoO = 3000 – 4000 ppm) display the weakest dependence of the initial permeability on temperature.

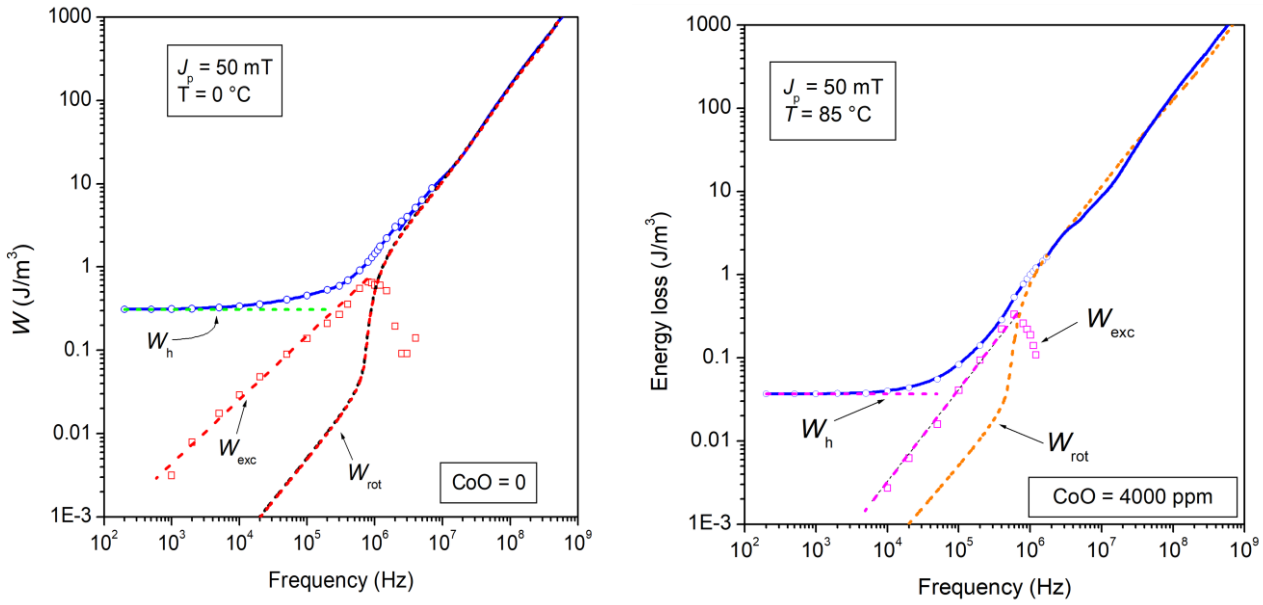

Figure S11. Examples of loss decomposition in samples with different CoO contents. The hysteresis loss W_h coincides with the limit of the measured loss $W(f)$ for $f \to 0$. The rotational loss $W_{rot}(f)$ is theoretically calculated by means of Eqs. (29) and (30). The dw generated excess loss $W_{exc}(f)$ is obtained by subtracting W_h and $W_{rot}(f)$ from $W(f)$. It is analytically expressed by Eq. (32) (dashed line).

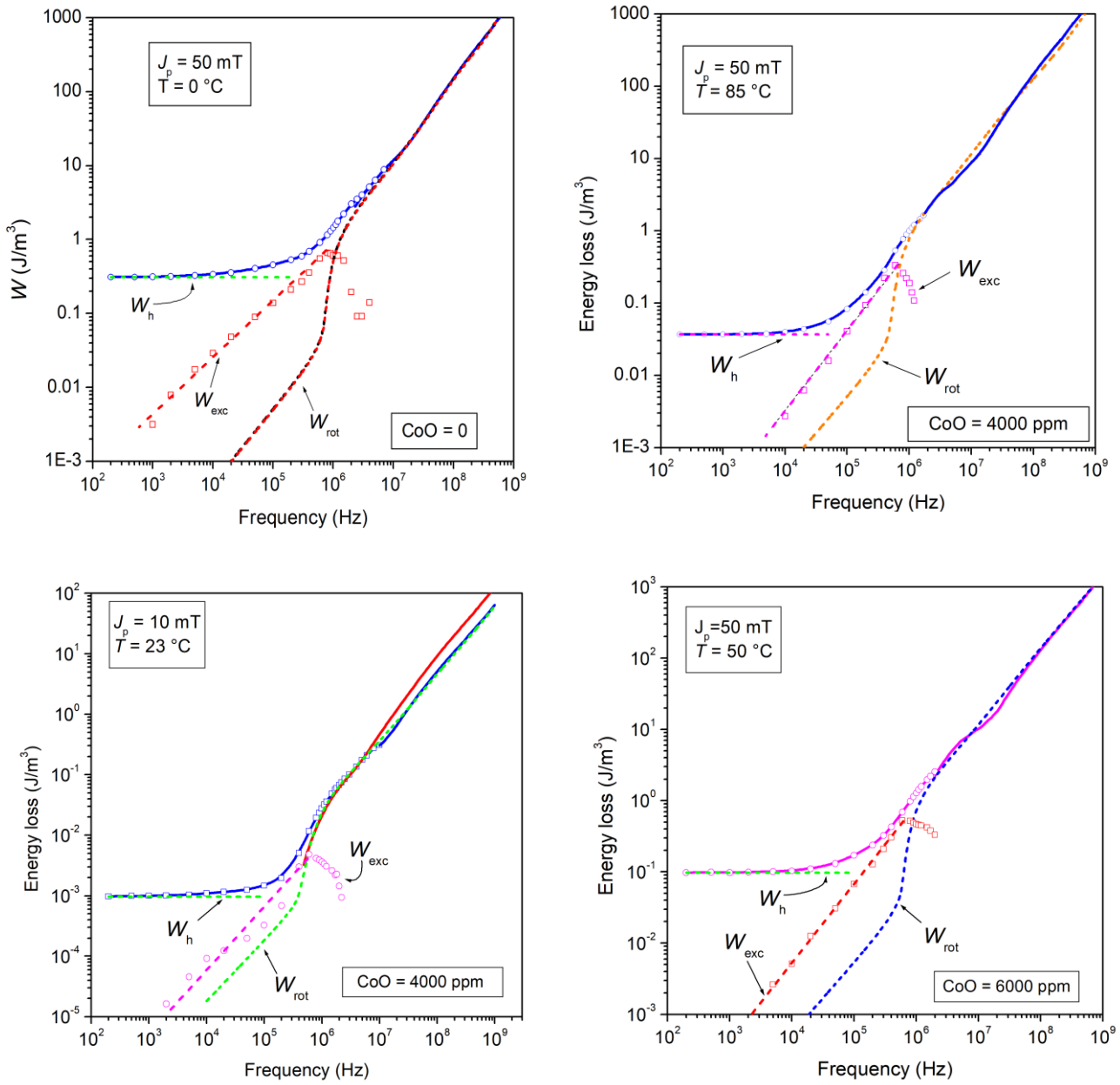

Figure S12. Loss decomposition in samples with different CoO contents. The hysteresis loss W_h coincides with the limit of the measured loss $W(f)$ for $f \to 0$. The rotational loss $W_{rot}(f)$ is calculated with Eq. (2), using the real and imaginary permeability components. The dw generated excess loss $W_{exc}(f)$ is obtained by subtracting W_h and $W_{rot}(f)$ from $W(f)$. It is analytically expressed by Eq. (32).